Muhamad Imam Firdaus[1], Ristiyanto Adiputra[2], Sharath Srinivasamurthy[3],*
*Aditya Rio Prabowo[4**], Faiz Nur Fauzi[5]*

DYNAMIC STABILITY ANALYSIS OF A TRIMARAN-TYPE FLOATING STRUCTURE WITH LARGE APPENDAGES

ANALIZA DINAMIČKE STABILNOSTI PLUTAJUĆE KONSTRUKCIJE TIPA TRIMARAN SA VELIKIM DODACIMA

Originalni naučni rad / Original scientific paper
Rad primljen / Paper received: 23.02.2026
https://doi.org/10.69644/ivk-2026-siA-0061
Adresa autora / Author's address:
[1)] Banten Merchant Polytechnic, Banten, Indonesia
M.I. Firdaus https://orcid.org/0000-0003-0539-0661
[2)] Research Center for Hydrodynamics Technology, National Research and Innovation Agency, South Tangerang, Indonesia
[*]email: ristiyanto.adiputra@brin.go.id
R. Adiputra https://orcid.org/0000-0003-3630-9432
[3)] Institute of Ocean Energy, Saga University, Saga, Japan
S. Srinivasamurthy https://orcid.org/0000-0001-9915-6301
[4)] Department of Mechanical Engineering, Universitas Sebelas Maret, Surakarta, Indonesia [**]email: aditya@ft.uns.ac.id ,
A.R. Prabowo https://orcid.org/0000-0001-5217-5943
[5)] Department of Ocean Engineering, Institut Teknologi Sepuluh Nopember, Surabaya, Indonesia
F.N. Fauzi https://orcid.org/0009-0002-5696-7934

Keywords
- ANSYS® AQWA
- floating structure
- boundary element method
- mooring system
- trimaran

Ključne reči
- ANSYS® AQWA
- plutajuća konstrukcija
- metoda graničnih elemenata
- sistem privezivanja
- trimaran

Abstract

Trimaran platforms provide enhanced stability and structural efficiency, making them attractive candidates for floating structures for marine energy systems. However, the integration of large appendages may alter the platform's hydrodynamic behaviour and influence mooring performance. This study investigates the dynamic response of a delta-trimaran floating platform designed to support an ocean-current turbine. The platform is stabilised by a spread mooring system, and four mooring configurations are evaluated: catenary, catenary-clump weight, soft-chain, and semi-taut. Two mooring line compositions are considered, namely chain-polyester rope-chain and chain-wire rope-chain. Coupled hydrodynamic simulations based on the boundary element method are performed using ANSYS® AQWA under combined environmental conditions. Platform motions, mean offsets, and mooring line tensions are analysed. Results show that soft-chain configurations produce the largest offsets, while the semi-taut system limits the mean offset to below 1 m. Peak mooring tensions range from 180 to 375 kN, remaining well below the minimum breaking load.

Izvod

Trimaranske platforme pružaju povećanu stabilnost i efikasne su konstrukcije, pogodne za plutajuće konstrukcije za pomorske energetske sisteme. Međutim, dodavanjem velikih privezaka dovodi se u pitanje hidrodinamičko ponašanje i uticaj na performanse sidrenja. U radu se istražuje dinamičko ponašanje plutajuće platforme delta trimarana, projektovane kao noseće konstrukcije turbine okeanskih strujanja. Platforma je stabilizovana sistemom raširenih veza, a data je procena četiri konfiguracije sidrenja: lančanom linijom, lančanom linijom sa otežanim tegovima, sa mekanim lancima i polunategnuti sistem sidrenja. Razmatraju se dva sastava užadi za privezivanje, tj. lanac-poliester uže-lanac i lanac-žičano uže-lanac. Obavljene su spregnute hidrodinamičke simulacije, na bazi metode graničnih elemenata korišćenjem ANSYS® AQWA u složenim uslovima okruženja. Analizirana su kretanja platforme, srednja odstupanja, kao i naprezanja vezova. Rezultati pokazuju da konfiguracije sidrenja mekanim lancima imaju najveća odstupanja, dok polunategnuti sistem ograničava srednje odstupanje ispod 1 m. Najveća zatezanja vezova su od 180 do 375 kN, što je znatno ispod minimalnog opterećenja prekida.

INTRODUCTION

Floating offshore structures must maintain structural integrity under continuous environmental loading, which can significantly influence platform stability, motion response, and station-keeping system performance /1, 2/. The interaction between the floating structure, the mooring system, and supported equipment governs the overall load distribution and structural behaviour of the system. In recent years, floating platforms are increasingly adopted in marine engineering applications, including support structures for renewable energy devices deployed in deeper waters where fixed-bottom solutions are not feasible, /3, 4/.

In such systems, the floating platform functions as the primary structural support /5/, while the mooring system maintains position and transfers environmental loads to the seabed. The platform response, including surge, sway, heave, roll, pitch, and yaw motions, governs stability and directly influences the loads experienced by mooring lines. Understanding these responses is therefore essential for evaluating the structural performance of floating systems. Among marine energy resources, ocean currents are considered promising due to their relatively steady, predictable flow, which enables continuous power generation. Global deployment of marine current technologies has expanded rapidly, with more than

500 MW installed and over 1600 MW planned, reflecting strong development momentum /6/. Depending on site conditions such as bathymetry and hydrodynamic environment, these systems may employ bottom-mounted /7/ or floating configurations /8/, where floating platforms offer installation flexibility, but introduce more complex interactions among the turbine, platform, and mooring system.

The structural response of floating platforms /9/, including surge, sway, heave, roll, pitch, and yaw motions, directly affects operational stability and the load experienced by mooring lines. Several studies have investigated floating platforms with different structural configurations and mooring arrangements. Ma et al. /10/ examines a catamaran platform equipped with a vertical axis turbine and shows that turbine rotation under environmental loading conditions increases mooring tension and contributes to larger lateral displacement as well as higher pitch, roll, and yaw responses. Similarly, Arini et al. /11/ validate a double-hull floating platform with catenary mooring and report that turbine operation produces higher mooring tension. At the same time, surge and pitch responses remain consistent with experimental data.

Other researchers focus on comparing different floating platform geometries. Guo et al. /12/ analyses a semi-submersible platform with prescribed six-degree-of-freedom motions (6 DOF), where surge and pitch motions dominate the torque and thrust spectra, with performance being most stable when the rotor is placed near the platform centre.

Despite these developments, comparative analyses that evaluate multiple mooring layouts and line-material combinations within a single floating platform configuration remain limited. Most previous work focuses on a single mooring type or structural arrangement, which limits understanding of how alternative station-keeping strategies affect platform motions and mooring load responses, particularly for multi-hull floating structures.

Therefore, this study investigates the structural response of a delta trimaran floating platform used as a support structure for an ocean current turbine. Four mooring layouts and two line-material compositions are analysed to evaluate their influence on platform motions and mooring line tensions. Numerical simulations are performed under combined environmental loading using the Boundary Element Method (BEM) implemented in ANSYS® AQWA. The analysis focuses on six-degree-of-freedom platform motions, mooring tension responses, and their peak and spectral characteristics to assess the structural performance of the floating system.

METHODOLOGY

This study follows a structured workflow, as shown in Fig. 1, comprising geometric modelling, hydrodynamic diffraction analysis, and frequency- and time-domain simulations using the BEM in ANSYS® AQWA. The delta-trimaran floating platform geometry is prepared and meshed based on previous studies. Hydrodynamic diffraction analysis is then conducted in the frequency domain under linear potential-flow assumptions /13/, and the numerical setup is validated by comparing hydrodynamic coefficients and motion responses with published results.

After validation, two vertical ocean-current turbines are added between the main hull and demi-hulls and are modelled as non-rotating components, represented only by additional mass and projected area. The simulations consider four mooring layouts: catenary, catenary with clump weight, soft-chain, and semi-taut, each with two line-material combinations. Combined wave and current loads from head, beam, and quartering sea directions are applied, and the outputs include 6 DOF motions, mooring line tensions, positional spectral density, and peak tension responses.

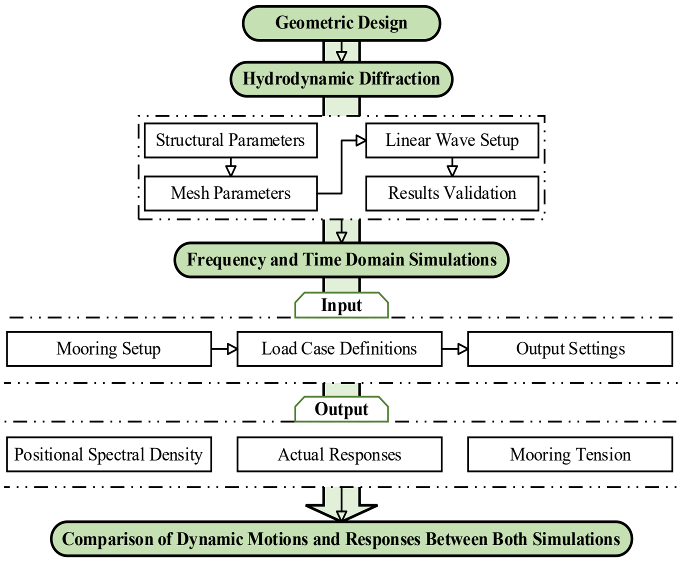

Figure 1. Research flowchart.

Theoretical basis

Hydrodynamic interaction between floating structures and waves can be solved numerically using BEM. By applying Green's function, the governing equations are converted into boundary integrals, reducing the problem dimension /14/. The discretised boundary then forms a linear system that can be solved efficiently. Several boundary conditions are applied as shown in Fig. 2.

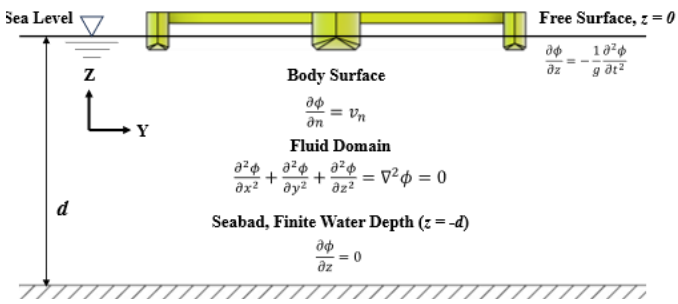

Figure 2. Boundary conditions.

After applying boundary conditions, the wave-structure interaction is evaluated using the total velocity potential. The fluid is assumed incompressible and irrotational, and a Green's function is used to solve the wave equation for an infinite-depth domain /15/. The resulting total potential ϕ is then used to assess the 6-DOF motion of the structure using the BEM formulation in Eq.(1).

In Eq.(1), M denotes structural mass, $A(\omega)$ is the added mass, $B(\omega)$ represents radiation damping, C is the restoring force term, $X(\omega)$ is frequency-dependent motion amplitude for the 6-DOF responses, and $F_{ext}(\omega)$ refers to the external excitation force.

Then, this study also examines the mooring system in which the hydrodynamic forces on each mooring line are calculated using the Morison equation, Eq.(2) /16-18/.

$$[-\omega^2(M + A(\omega)) + I\omega B(\omega) + C]X(\omega) = F_{ext}(\omega), \qquad (1)$$

$$F(X,Z,t) = \frac{\rho\pi D^2 \ddot{u}_x}{4} + \frac{C_m \rho\pi D^2 (\ddot{u}_x - \ddot{u}_t)}{4} + 0.5 C_d \rho D(\dot{u}_x - \dot{u}_t)|\dot{u}_x - \dot{u}_t| \, . \qquad (2)$$

In Eq.(2), $\dot{u}_x$ and $\ddot{u}_x$ represent the water particle velocity and acceleration in the in-line direction, while $\dot{u}_t$ and $\ddot{u}_t$ denote the cylinder's corresponding velocity and acceleration. Parameters ρ and D refer to the water density and cylinder diameter, consecutively. C_m and C_d are the inertia and drag coefficients, consecutively. The values of inertia and drag coefficients are taken from the literature and incorporated into the mooring-line hydrodynamic properties.

Within this theoretical framework, the hydrodynamic formulation is based on linear potential flow theory in the frequency domain. Higher-order wave excitation effects, including second-order quadratic transfer functions (QTFs), as well as viscous damping effects, are not considered within the scope of this study. Accordingly, the resulting motion responses and hydrodynamic loads should be interpreted as first-order estimates appropriate for preliminary engineering assessment.

Validation and benchmarking

For validation and benchmarking, this study refers to a previous numerical investigation that examines the distance or gap between the main hull and the side hull, /19/. From that work, one configuration is selected for further analysis in this study (see Fig. 3). The main parameters of the ship are summarised in Table 1.

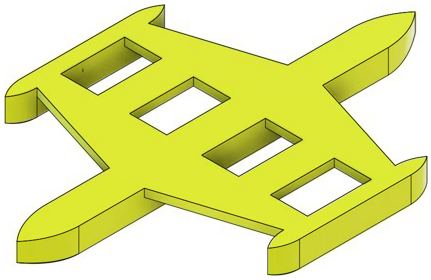

Figure 3. Delta trimaran design, /19/.

Table 1. Main parameters of the floater, /19/.

Parameters	Value
Length (L)	25 m
Main Hull Beam (B_m)	2.2 m
Demi Hull Beam (B_d)	1.1 m
Draft (D)	0.55 m
Height (H)	1.7 m
Centre of gravity (x, y, z)	(0.0 m, 0.0 m, 0.0 m)
Ship mass	36843 kg
Radius of gyration (x, y, z)	(6.00 m, 6.25 m, 6.50 m)

The incident wave is set as a quartering sea condition (45°), and the results are presented in Fig. 5. The comparison is performed using response amplitude operators (RAOs) for heave, roll, and pitch motions. The present results show good agreement with the previous study, with differences of less than 5 %. Based on this validation, the numerical setup is considered reliable, and the simulations can be continued to the case configuration stage for further analysis.

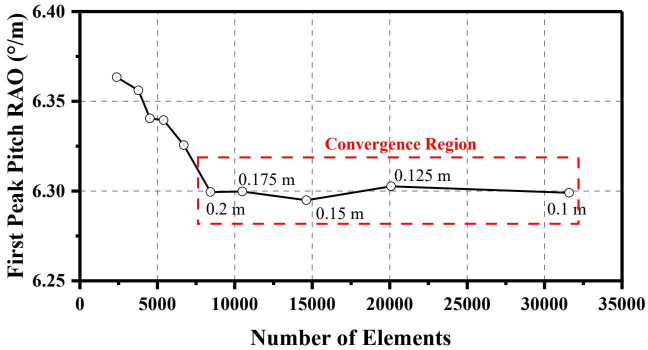

Figure 4. Mesh convergence.

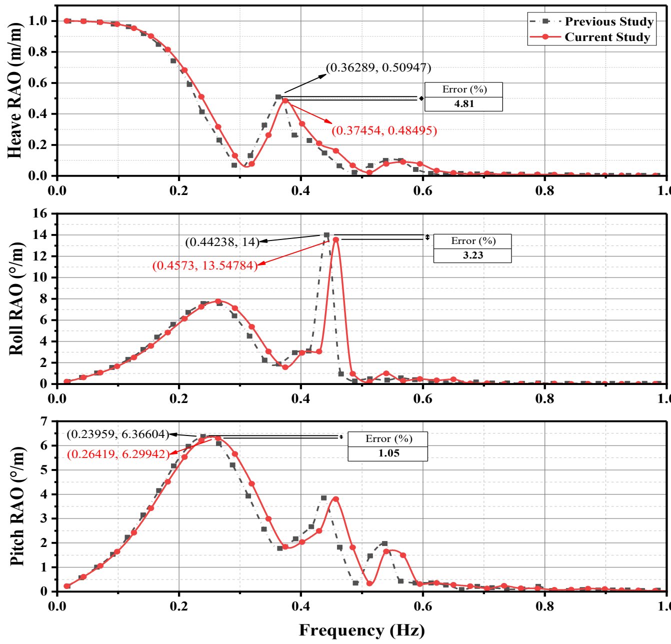

Figure 5. Validation of results.

CASE CONFIGURATIONS

Floating structure

The validated delta-trimaran design is modified by adding a pair of turbines between the main hull and the side hull, as shown in Fig. 6. The turbines are modelled as non-rotating components and represented through their added mass and projected area to account for inertial and hydrodynamic resistance effects. This modification increases the total mass to 38276.68 kg and shifts the vertical centre of gravity from 0 to –0.025 m relative to the draft, which is sufficient to represent the added load in the motion response simulations. Under this representation, turbine rotational dynamics and thrust-induced load variations are not explicitly represented, and the predicted motion and mooring responses reflect a simplified modelling assumption appropriate for preliminary analysis.

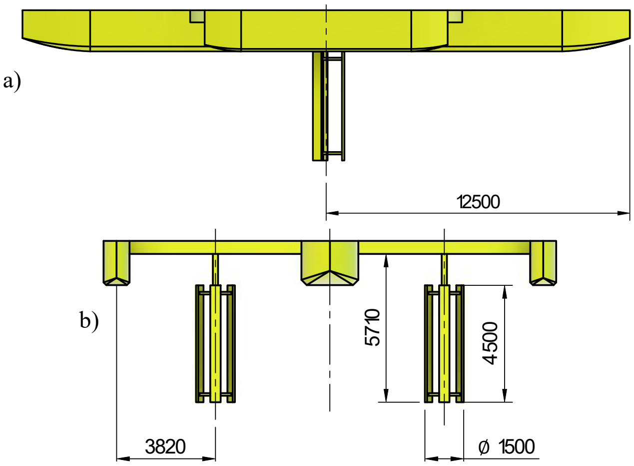

Figure 6. Delta-trimaran equipped with twin turbines: a) side view; b) front view.

Mooring system configuration

The floating ocean current platform employs a symmetric spread mooring system with four lines attached to the ends of the main hull (Fig. 7). This configuration provides balanced horizontal restoring forces, limits yaw motion, and maintains a stable heading relative to the incoming current, which is important for turbine operation, /20/.

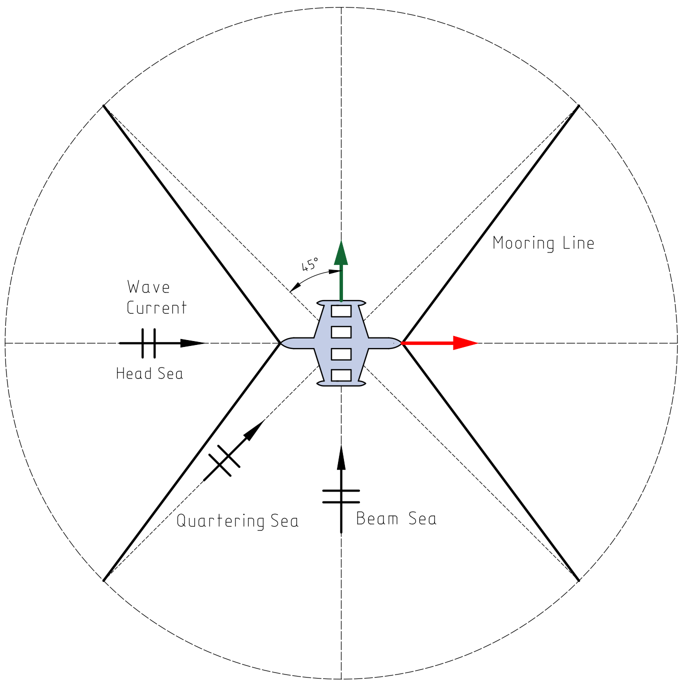

Figure 7. Spread mooring configuration.

As illustrated in Fig. 7, four mooring configurations are examined: catenary, catenary with clump weight, soft-chain, and semi-taut. Each line consists of three segments, with the middle section made of polyester or wire rope to control axial stiffness and tension while reducing excessive weight compared to all-chain systems, /21/.

The catenary system offers high flexibility and horizontal restoring capability, /22/, while the addition of a clump weight improves vertical restoring forces. The soft-chain configuration, adapted from Lee and Ong /23/, combines catenary and semi-taut features by using a partially seabed-resting chain and a buoy-supported polyester rope to reduce abrasion and smooth out tension variations. The semi-taut system uses a short top chain, a polyester rope, a ground chain, and a subsea buoy to balance flexibility and stiffness, resulting in improved heading control and positional stability, /24/.

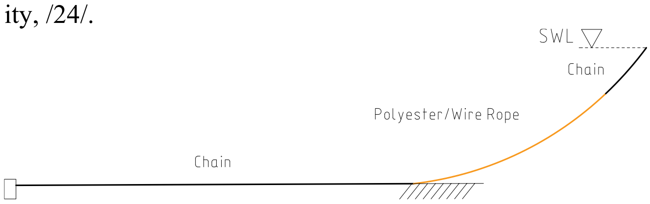

(a) Catenary

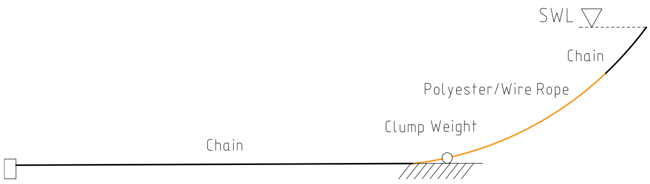

(b) Catenary-clump weight

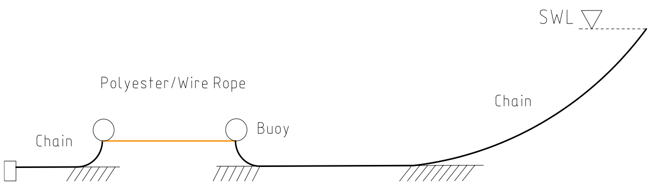

(c) Soft-chain

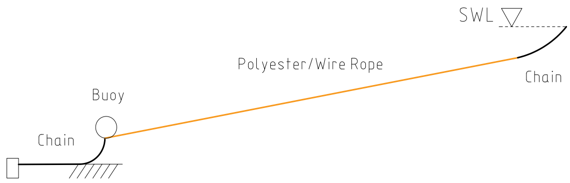

(d) Semi-taut

Figure 8. Mooring line configurations.

The material properties of the mooring components used in this study are listed in Tables 2 and 3. For the four mooring configurations, the anchor radius is determined based on water depth. According to Ma et al. /25/, a depth of 50 m corresponds to an anchor radius of approximately eight times the depth, which is applied to all configurations except the semi-taut system. For the semi-taut configuration, a fixed anchor radius of 300 m is used. The detailed setup for each mooring-line configuration is provided in Table 4.

Table 2. Material properties.

Properties	Chain /26/	Polyester rope /27/	Wire rope /25/
Mass	126 kg/m	13.3 kg/m	27.36 kg/m
Cross-section area	0.0045 m^2	0.0107 m^2	0.0049 m^2
Stiffness, *EA*	6300 MN	20.16 MN	553.5 MN
MBL	4.8843 MN	3.42 MN	5.617 MN
Added mass coeff.	1	1	1
Transverse drag coeff.	2.4	1	1
Equivalent diam.	0.076 m	0.117 m	0.079 m
Longitud. drag coeff.	1.15	0.1	0.1

Table 3. Bouy and clump weight properties.

Properties	Buoy /28/	Clump weight /29/
Mass	800 kg	5000 kg
Displaced mass	4000 kg	652 kg
Added mass	2000 kg	652 kg
Drag coeff. × area	1.486 m^2	0.81 m^2

Table 4. Mooring design.

Mooring	Section length (m)	Location, *xyz* (m)	Pre-tension by mid-section type (kN)
Catenary	1 = 274; 2 = 100; 3 = 30	Fairlead = (± 9.715, ±1.1, 0.5) Anchor = (± 282.84, ±282.84, -50)	polyester = 35.572; wire = 66.194
Catenary-clump weight	1 = 274; 2 = 100; 3 = 30	Fairlead = (± 9.715, ±1.1, 0.5) Anchor = (± 282.84, ±282.84, -50)	polyester = 39.403; wire = 73.985
Soft-chain	1 = 75; 2 = 115; 3 = 230	Fairlead = (± 9.715, ±1.1, 0.5) Anchor = (± 282.84, ±282.84, -50)	polyester = 40.021; wire = 36.018
Semi-taut	1 = 75; 2 = 192; 3 = 30	Fairlead = (± 9.715, ±1.1, 0.5) Anchor = (± 212.13, ±212.13, -50)	polyester = 95.719; wire =180.806

Simulation settings

A summary of the environmental conditions and time-domain simulation parameters is provided in Table 5.

Table 5. Simulation settings.

Parameters	Details
wave /30/	JONSWAP spectrum Significant wave height (H_s) = 1.5 m Peak period (T_p) = 6.0 s Peak enhancement factor (γ) = 1.2 Directions = head, beam, and quartering
current /30/	Current speed = 1.5 m/s Constant over all depths Direction follows the wave direction
simulation duration	10800 s (3 hours)
statistical time window	10800 s (3 hours) used to compute statistics and maxima

Summarised cases

Table 6 summarises all simulation cases, where variations in wave and current directions across all mooring-line types result in 24 distinct configurations.

Table 6. Case configurations.

No	Parameters and symbols
1	Incident wave-current direction: head sea (1a); beam sea (1b); and quartering sea (1c)
2	Catenary: chain-polyester rope-chain (2a) and chain-wire rope -chain (2b)
3	Catenary-clump weight: chain-polyester rope-chain (3a) and chain-wire rope-chain (3b)
4	Soft-chain: chain-polyester rope-chain (4a) and chain-wire rope-chain (4b)
5	Semi-taut: chain-polyester rope-chain (5a) and chain-wire rope-chain (5b)

RESULTS AND DISCUSSION

Motion spectral density

Position Spectral Density (PSD) analysis is used to assess the frequency-domain response of the floating structure under wave–current excitation. The results indicate that the natural frequencies of the structure and mooring system consistently fall within 0.18-0.22 Hz.

Under head sea wave-current conditions (see Fig. 9), the surge PSD results show that the mooring configuration and mid-section material mainly affect the peak magnitude. The soft-chain configuration produces the highest surge peak of about 1.26 m^2/Hz due to its more compliant behaviour and lower horizontal restoring force, whereas the semi-taut system, with higher pre-tension and stiffness, results in the lowest peak at approximately 0.14 m^2/Hz.

The addition of a clump weight to the catenary system slightly reduces the surge peak, suggesting improved restoring force and damping performance, whereas the effect of material variation between polyester and wire rope is relatively small. For pitch motion, a similar ranking is observed, with the soft-chain configuration showing the largest peak of around 36 $°^2$/Hz, while the other configurations exhibit comparable values within the range of 20-23 $°^2$/Hz, indicating that pitch response is less sensitive to mooring variations than surge.

For beam sea conditions (Fig. 10), the PSD characteristics of sway and roll follow the same overall response tendency as previously identified for surge and pitch under head sea excitation, although with distinct motion-specific features. Changes in mooring configuration mainly alter the magnitude of the spectral peaks, while the associated dominant frequencies remain nearly unchanged among the investigated cases.

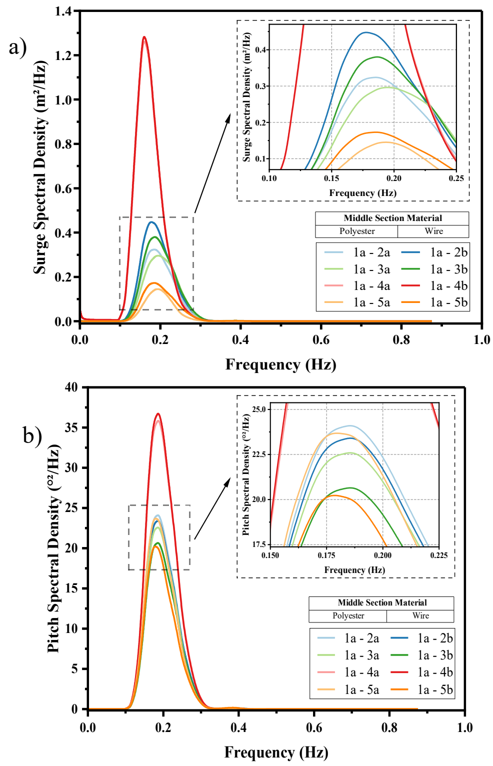

Figure 9. Spectral density for head seas: a) surge; b) pitch.

The soft-chain system consistently produces the largest sway and roll responses, reflecting its higher lateral compliance and reduced restoring stiffness, whereas the semi-taut configuration results in the lowest spectral peaks due to its higher pre-tension and stronger motion restraint. Compared to pitch motion, the roll response exhibits significantly higher PSD peaks, reaching nearly twice the magnitude, which can be attributed to the larger roll RAO of the floating structure under beam-sea loading.

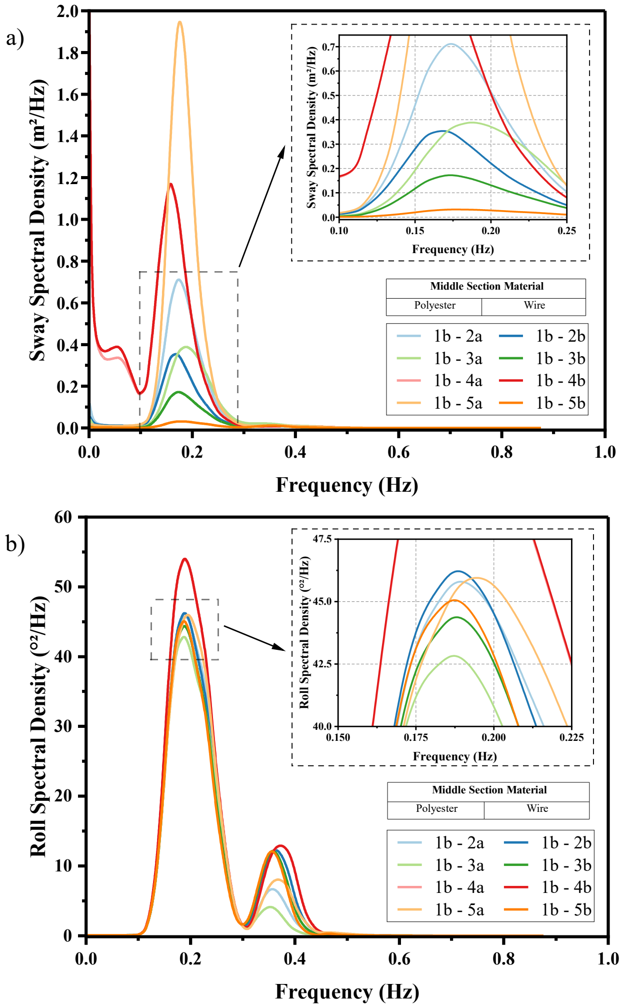

Figure 10. Spectral density for beam seas: a) sway; b) roll.

In quartering sea conditions (Fig. 11), the heave PSD exhibits very limited sensitivity to variations in mooring configuration and mid-section material, with peak values consistently ranging between approximately 0.9 and 1.0 m^2/Hz, indicating that heave motion is mainly governed by the vertical hydrodynamic characteristics of the floating structure.

A similar overall tendency is observed for yaw motion; however, a pronounced maximum yaw PSD of about 11.8 $°^2$/Hz occurs for configuration 1c-4b. This elevated response is associated with a slack mooring condition, as indicated by the pre-tension values in Table 4, where the heavier wire-rope mid-section prevents the buoy from maintaining sufficient tension. The remaining configurations follow response trends consistent with those observed for the other motion components, confirming that the mooring configuration primarily influences the response magnitude rather than the dominant frequency.

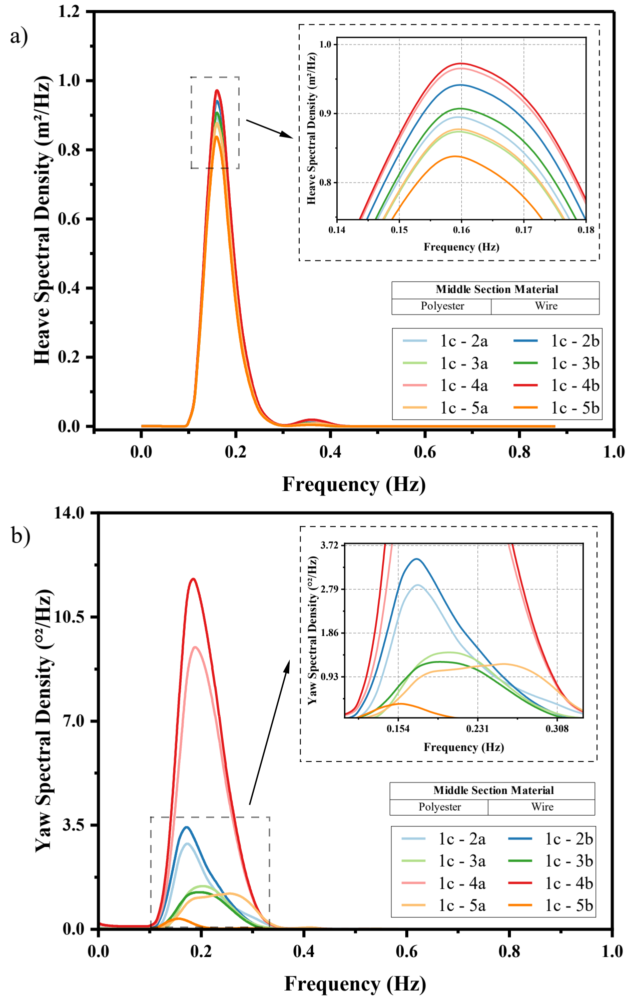

Figure 11. Spectral density for quartering seas: a) heave; b) yaw.

Actual responses in irregular wave

In the irregular wave analysis, simulations are performed for 10800 s, while only the first 1000 s are shown for clarity. The time-domain responses and statistical results for surge and pitch under head sea conditions are presented in Fig. 12 and summarised in Table 7.

The soft-chain mooring system exhibits a significant surge offset, with a maximum of approximately 15 m and a mean of approximately 14 m, due to its low horizontal restoring stiffness arising from the buoy-supported mid-section and limited seabed contact. In contrast, the semi-taut configuration, which has the highest pre-tension and a shorter anchor radius, results in the smallest surge offset, with mean values below 1 m.

As pre-tension decreases from semi-taut to catenary with clump weight and conventional catenary systems, the surge response increases, showing the combined influence of mooring stiffness. The clump weight increases line mass and damping, affecting the surge behaviour. Configurations with wire rope exhibit more restrained surge motions than those with polyester rope due to the higher axial stiffness of wire rope. Pitch responses are similar across configurations, ranging from about +5° to −7°, with the soft-chain system producing the largest absolute pitch motion. The negative values in Table 7 indicate the direction of rotation rather than the response magnitude, and this convention is also applied to all rotational motions.

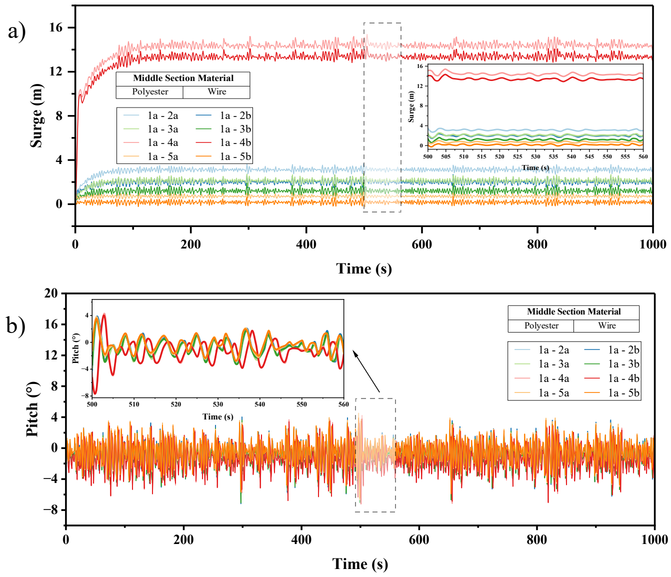

Figure 12. Time domain responses for head seas: a) surge (head sea); b) pitch (head sea).

Table 1. Statistics of head sea responses.

Motion	Case	Mean	Std. dev.	Max	Min
Surge (m)	1a - 2a	3.12	0.17	3.71	0.00
	1a - 2b	2.02	0.21	2.77	0.00
	1a - 3a	2.12	0.19	2.83	0.00
	1a - 3b	1.20	0.20	2.01	0.00
	1a - 4a	14.39	0.38	15.77	0.00
	1a - 4b	13.36	0.36	14.67	0.00
	1a - 5a	0.71	0.12	1.25	0.00
	1a - 5b	0.17	0.15	0.75	0.00
Pitch (°)	1a - 2a	-0.80	1.67	5.16	-7.02
	1a - 2b	-0.76	1.75	5.40	-7.66
	1a - 3a	-0.93	1.63	4.87	-7.28
	1a - 3b	-0.88	1.67	4.92	-7.60
	1a - 4a	-1.34	1.82	5.90	-8.32
	1a - 4b	-1.35	1.82	5.46	-8.41
	1a - 5a	-0.44	1.62	5.57	-7.28

Figure 13 and Table 8 show the time domain responses and statistical characteristics of sway and roll under beam-sea conditions. The sway response strongly depends on the mooring configuration, following a trend similar to surge under head sea excitation. The soft-chain system produces the largest sway, with mean values around 14 m and a maximum of about 16.6 m. At the same time, the semi-taut configuration yields the smallest response, with mean values below 1 m and maxima generally under 2.5 m. The catenary and catenary-clump weight systems show intermediate sway responses, with mean values of approximately 1-3 m.

Differences related to mid-section material are relatively small; however, wire rope cases consistently show slightly lower mean and maximum sway values than polyester rope. In contrast, roll motion exhibits smaller variations among configurations, with maximum roll angles for most cases lying within the range of 10-12° and minimal values around −10°, indicating that roll response is less sensitive to mooring configuration and follows the same general tendency observed in the previous head-sea analysis.

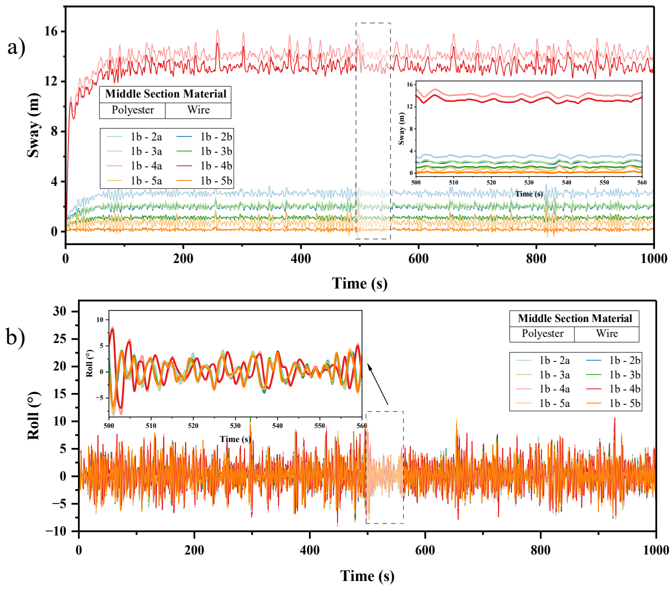

Figure 13. Time domain responses for beam sea: a) sway; b) roll.

Table 8. Statistics of beam sea responses.

Motion	Case	Mean	Std. dev.	Max	Min
Sway (m)	1b - 2a	3.06	0.21	4.23	0.00
	1b - 2b	1.97	0.16	2.72	0.00
	1b - 3a	2.05	0.20	3.07	0.00
	1a - 3b	1.13	0.12	1.80	0.00
	1b - 4a	14.20	0.53	16.59	0.00
	1b - 4b	13.21	0.50	15.61	0.00
	1b - 5a	0.72	0.32	2.34	0.00
	1b - 5b	0.16	0.08	0.55	0.00
Roll (°)	1b - 2a	0.28	2.72	10.82	-9.20
	1b - 2b	0.27	2.75	11.89	-9.85
	1b - 3a	0.31	2.69	11.11	-9.93
	1a - 3b	0.31	2.74	11.84	-10.50
	1b - 4a	0.41	2.89	10.48	-11.11
	1b - 4b	0.41	2.86	10.67	-10.94
	1b - 5a	0.19	2.76	11.00	-10.82

The quartering sea responses of heave and yaw motions are illustrated in Fig. 14 and summarised in Table 9. Heave motion shows nearly uniform behaviour across all mooring configurations, with mean values between approximately −0.34 and −0.63 m and maximal values ranging from about 0.47 to 0.65 m, indicating limited sensitivity to mooring layout and mid-section material.

In contrast, yaw motion exhibits a stronger dependence on the mooring configuration. The semi-taut and soft-chain systems effectively limit yaw motion, with mean values close to zero and maximal values generally below 6°, whereas the conventional catenary and catenary-clump weight configurations result in substantially larger yaw responses, with mean values of approximately −10 to −14° and minimum values reaching about −16°. Addition of a clump weight provides a modest reduction in yaw response, while the influence of mid-section material remains relatively small. This trend is associated with the lower restoring moment about the vertical axis in catenary-based systems under quartering sea excitation.

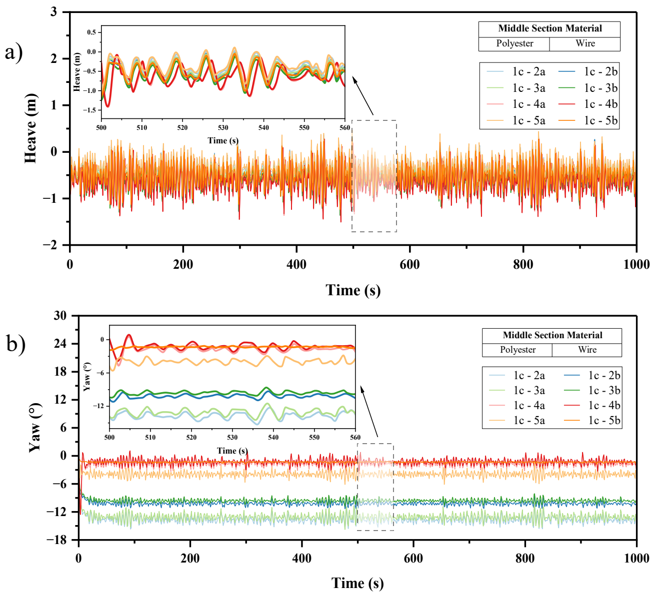

Figure 14. Time domain responses for quartering sea: a) heave; b) yaw.

Table 9. Statistics of quartering sea responses.

Motion	Case	Mean	Std. dev.	Max	Min
Heave (m)	1c - 2a	-0.39	0.25	0.60	-1.35
	1c - 2b	-0.49	0.27	0.60	-1.49
	1c - 3a	-0.46	0.24	0.51	-1.41
	1c - 3b	-0.57	0.26	0.52	-1.49
	1c - 4a	-0.63	0.27	0.47	-1.58
	1c - 4b	-0.62	0.28	0.47	-1.60
	1c - 5a	-0.34	0.25	0.65	-1.33
	1c - 5b	-0.51	0.25	0.49	-1.46
Yaw (°)	1c - 2a	-13.69	0.70	-7.71	-16.69
	1c - 2b	-10.22	0.39	-3.35	-12.06
	1c - 3a	-13.09	0.76	-8.72	-16.05
	1c - 3b	-9.59	0.37	-3.75	-11.01
	1c - 4a	-1.68	0.68	1.82	-12.56
	1c - 4b	-1.26	0.64	1.72	-12.55
	1c - 5a	-3.94	0.60	-0.82	-6.82

Mooring line tension

The maximum tension of individual mooring lines under head sea conditions is presented in Fig. 15. The highest peak tension occurs in the semi-taut configuration with a wire-rope mid-section, reaching about 300 kN, consistent with its high pre-tension and shorter anchor radius. In contrast, the semi-taut configuration with a polyester mid-section exhibits a much lower maximal tension of around 180 kN, comparable to catenary-based systems, due to the higher axial compliance of polyester rope that limits peak load despite high pre-tension.

Catenary and catenary-clump weight systems generally show lower tensions because of their compliant geometry, although the clump weight slightly increases the maximum values to about 180-270 kN. The soft-chain configuration yields intermediate tension levels due to buoy-induced load redistribution, despite producing relatively large translational offsets. Differences among individual lines are evident: lines aligned with the incoming wave-current direction carry higher loads, while wire rope generally results in higher peak tensions than polyester rope.

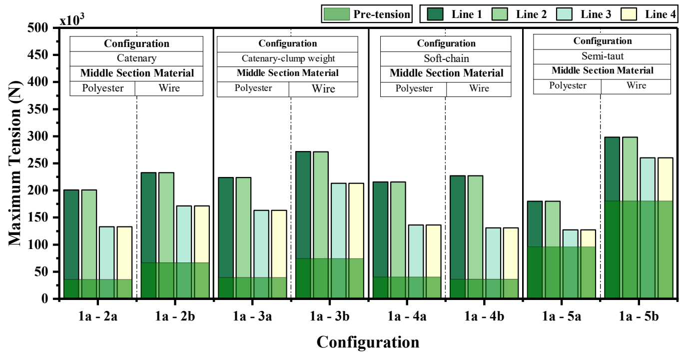

Figure 1. Maximum mooring system tension in head sea.

For beam-sea conditions, the maximal mooring line tensions for each configuration are presented in Fig. 16. The overall trend is similar to that observed under head sea excitation; however, higher peak values are recorded. In particular, configurations 1b-5b reach maximal tensions of approximately 375 kN, while the remaining configurations generally fall within the 250-300 kN range. The highest tensions consistently occur in Lines 1 and 4, which are aligned with the beam sea wave–current direction.

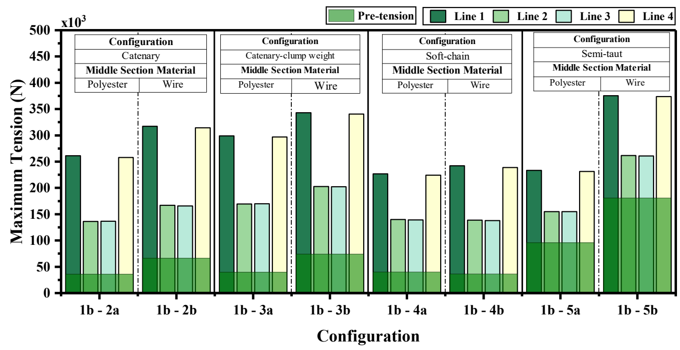

Figure 16. Maximum mooring system tension in beam sea.

The maximum mooring line tensions under quartering-sea conditions are shown in Fig. 17. For the catenary system, the highest tensions occur in Lines 1, 2, and 4, with peak values ranging from approximately 200 to 300 kN. The inclusion of a clump weight slightly increases the maximum tension, while wire-rope cases consistently produce higher values than polyester rope. For the semi-taut system, the maximum tension is mainly concentrated in Line 1, whereas Lines 2 and 4 exhibit similar tension levels due to their symmetric orientation relative to the quartering wave-current direction. For both materials, the semi-taut configuration with a poly

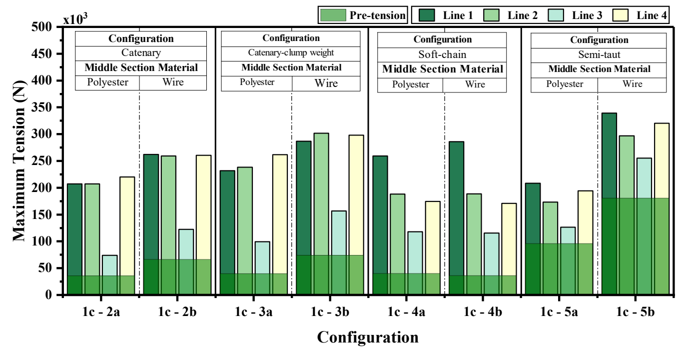

Figure 17. Maximum mooring system tension in quartering sea.

ester mid-section exhibits maximum tensions in Line 1 of about 260 kN, comparable to those in the catenary system.

In contrast, the semi-taut system with wire rope maintains the highest peak tension, reaching approximately 350 kN in Line 1. Overall, the maximum tensions for all wave-current directions remain well below the Minimum Breaking Load (MBL), indicating that the mooring system operates safely under the investigated environmental conditions.

CONCLUSIONS

This study examines the dynamic response of a delta trimaran floating ocean current platform under combined wave and current excitation using four mooring layouts and two mid-section materials. The results confirm that mooring configuration and pretension level are the primary factors controlling translational motions and mooring line tensions. In contrast, rotational motions are primarily governed by the platform's hydrodynamic characteristics. Frequency-domain analysis further shows that dominant response frequencies remain similar for all configurations, indicating that wave characteristics control the response frequency, whereas the mooring system determines the response magnitude.

Soft-chain configurations generate the largest surge and sway offsets, reaching approximately 14-16 m due to their high compliance. Semi-taut systems provide the most effective motion control, limiting mean offsets to below 1 m, but produce higher peak mooring line tensions, particularly when wire rope is used. The addition of clump weight slightly improves motion restraint in catenary systems while increasing line tension. All configurations remain well below the minimum breaking load, indicating safe performance under the investigated environmental conditions.

In the context of the motion and mooring responses discussed above, viscous damping is recognised as an important mechanism influencing resonant motions and, consequently, peak mooring line tensions, as highlighted in design guidelines such as DNV-OS-E301. Within the linear potential-flow framework adopted in this study, the reported maximal mooring tensions therefore represent first-order estimates of the system response. To further enhance the fidelity of motion and mooring response predictions, future studies may extend the present framework by incorporating linearised viscous damping effects. In addition, the inclusion of second-order wave effects, such as mean drift forces and low-frequency quadratic transfer functions, as well as wave-current directional misalignment, would enable a more comprehensive assessment of slow-drift motions and extreme mooring loads. Furthermore, future work may consider turbine representations with variable rotational speed as a function of current velocity to better capture turbine-platform coupling effects and their influence on dynamic responses and mooring loads.

ACKNOWLEDGEMENT

This research is based on results from the Joint Research of Ocean Energy programme conducted with the Institute of Ocean Energy at Saga University. The authors would like to express their sincere appreciation to the Institute of Ocean Energy at Saga University for its support.

REFERENCES

1. Diatmaja, H., Prabowo, A.R., Adiputra, R., et al. (2023), *Comparative evaluation of design variations in prototype fast boats: A hydrodynamic characteristic-based approach*, Math. Model. Eng. Probl. 10(5): 1487-1507. doi: 10.18280/mmep.100501
2. Pratama, A.S., Prabowo, A.R., Tuswan, T., et al. (2023), *Fast patrol boat hull design concepts on hydrodynamic performances and survivability evaluation*, J Appl. Eng. Sci. 21(2): 501-531. doi: 10.5937/jaes0-40698
3. Budisetyawan, D., Fauzi, F.N., Adiputra, R., et al. (2025), *Wind turbine reliability forecast: A technical review on the research milestone and assessment of the energy cost using Monte Carlo simulation*, Eng. Sci. 35: 1502. doi: 10.30919/es1502
4. Fauzi, F.N., Puryantini, N., Prabowo, A.R., et al. (2024), *Implementation assessment of the offshore wind turbine (OWT) for remote regions' electrification in Indonesia based on geographical potential and economic attractiveness*, Eng. Sci. 32: 1295. doi: 10.30919/es1295
5. Julianto, R.I., Muttaqie, T., Adiputra, R., et al. (2020), *Hydrodynamic and structural investigations of catamaran design*, Procedia Struct. Integr. 27: 93-100. doi: 10.1016/j.prostr.2020.07.013
6. Febrianto, R.A., Prabowo, A.R., Baek, S.J., Adiputra, R. (2021), *Analysis of monohull design characteristics as supporting vessel for the COVID-19 medical treatment and logistic*, Transp. Res. Procedia 55: 699-706. doi: 10.1016/j.trpro.2021.07.038
7. Kraedegh, A.M., Jeremić, L., Martić, I., et al. (2024), *Integrity and risk assessment of offshore jacket structures*, Struct. Integr. Life, 24(3): 380-385. doi: 10.69644/ivk-2024-03-0380
8. Sreenivasan, H., Krishna, S., Rao, M.H.V.R., Vij, R.K. (2021), *Postulated failure analyses of tension leg platform (TLP) restraining system under the influence of varying sea-state condition*, Struct. Integr. Life, Spec. Issue, 21: S29-S37
9. Yang, Z., Ren, Z., Li, Z., et al. (2022), *A comprehensive analysis method for levelized cost of energy in tidal current power generation farms*, Renew. Energy, 182: 982-991. doi: 10.1016/j.renene.2021.11.026
10. Ma, Y., Li, T.-F., Zhang, L., et al. (2016), *Experimental study on hydrodynamic characteristics of vertical-axis floating tidal current energy power generation device*, China Ocean Eng. 30(5): 749-762. doi: 10.1007/s13344-016-1001-y
11. Arini, N.R., Thies, P.R., Johanning, L., et al. (2019), *Feasibility study of mooring lines design for a floating tidal turbine platform using double hull structure*, In: Proc. Int. Conf. Offshore Mech. Arct. Eng. - OMAE, Glasgow, Scotland, 2019, Vol.10: OMAE2019-95998, V010T09A007. doi: 10.1115/OMAE2019-95998
12. Guo, X., Yang, J., Lu, W., Li, X. (2018), *Dynamic responses of a floating tidal turbine with 6-DOF prescribed floater motions*, Ocean Eng. 165: 426-437. doi: 10.1016/j.oceaneng.2018.07.017
13. Firdaus, M.I., Firdaus, N., Adiputra, R., Alfajar, M. (2025), *Hydrodynamics of spar-type floating offshore wind turbine under variation of mooring system configuration*, In: M.L. Kolhe (Ed.), Proc. 15th Int. Conf. on Renewable and Clean Energy (ICRCE 2025), Lecture Notes in Electrical Eng., vol. 1434: 85-92. Springer, Singapore, 2025. doi: 10.1007/978-981-96-8154-9_10
14. Adiputra, R., Firdaus, M.I., Firdaus, N., et al. (2025), *Hydrodynamic responses of OTEC floating platform in operating and dismantling states*, In: M.L. Kolhe (Ed.), Proc. 15th Int. Conf. on Renewable and Clean Energy (ICRCE 2025), Lecture Notes in Electrical Eng., vol. 1434: 69-76. Springer, Singapore, 2025. doi: 10.1007/978-981-96-8154-9_8
15. Adiputra, R., Fauzi, F.N., Firdaus, N., et al. (2023), *Roundness and slenderness effects on the dynamic characteristics of spar-type floating offshore wind turbine*, Curved Layer. Struct. 10 (1): 20220213. doi: 10.1515/cls-2022-0213

16. Fauzi, F.N., Satrio, D., Adiputra, R. (2026), *Hydrodynamic responses of floating oscillating water column for wave energy conversion*, E3S Web Conf., 687: 01010. doi: 10.1051/e3sconf/202668701010
17. Krishna, S., Sreenivasan, H., Rao, M.H.V.R., Vij, R.K. (2021), *Dynamic analyses of a tension leg platform (TLP) under very rough sea-state*, Struct. Integr. Life, 21, Spec. Issue: S39-S44.
18. Fauzi, F.N., Adiputra, R., Firdaus, N., Prabowo, A.R. (2024), *Comparative study of wave forces on a spar-type FOWT under free floating conditions: The role of slenderness*, In: Salim, M.A., Khashi'ie, N.S., Chew, K.W., Photong, C. (Eds), Proc. 9th Int. Conf. and Exhibition on Sustainable Energy and Advanced Materials (ICE-SEAM 2023), Lecture Notes in Mech. Eng., Springer, Singapore, 2024: 615-619. doi: 10.1007/978-981-97-0106-3_97
19. Adiputra, R., Budisetyawan, D., Firdaus, N., et al. (2024), *Dynamic characteristics of trimaran type floating ocean current power plant*, In: 2024 Int. Conf. on Technology and Policy in Energy and Electric Power (ICTPEP 2024), Bali, Indonesia, 2024. doi: 10.1109/ICT-PEP63827.2024.10733472
20. Faizatama, A.M., Firdaus, N., Adiputra, R., et al. (2025), *Mooring stress analysis of OC3-Hywind floating platform with variation anchor placement*, Struc. Integr. Life, 25(2): 193-202. doi: 10.69644/ivk-2025-02-0193
21. Lian, Y., Zhong, F., Zheng, J., et al. (2023), *Effects of mooring line with different materials on the dynamic response of offshore floating wind turbine*, J Mar. Sci. Eng. 11(12): 2302. doi: 10.3390/jmse11122302
22. Faizatama, A.M., Firdaus, N., Adiputra, R., et al. (2025), *Hydrodynamic impact of cold-water pipes and mooring systems on KVLCC2 for floating OTEC platforms*, Ocean Eng. 341(Part 2): 122491. doi: 10.1016/j.oceaneng.2025.122491
23. Lee, C.F., Ong, M.C. (2025), *Numerical analysis of mooring systems for reducing peak mooring line tensions in a combined wind and wave energy system at an intermediate water depth*, Ocean Eng. 325: 120767. doi: 10.1016/j.oceaneng.2025.120767
24. Tang, H.-J., Ong, M.C., Hsu, T.-W. (2024), *Dynamic analysis of a 15 MW semi-taut mooring floating offshore wind turbine at intermediate water depth: Investigating mooring line failure under operating and parked conditions*, Ocean Eng. 312(Part 3): 119108. doi: 10.1016/j.oceaneng.2024.119108
25. Ma, K.-T., Luo, Y., Kwan, T., Wu, Y., Mooring System Engineering for Offshore Structures, Gulf Prof. Publ. 2019. doi: 10.1016/C2018-0-02217-3
26. Pols, A., Gubesch, E., Abdussamie, N., et al. (2021), *Mooring analysis of a floating OWC wave energy converter*, J Mar. Sci. Eng. 9(2): 228. doi: 10.3390/jmse9020228
27. Ghigo, A., Niosi, F., Paduano, B., et al. (2022), *Mooring system design and analysis for a floating offshore wind turbine in Pantelleria*, In: Proc. ASME Turbo Expo: Turbomachinery Technical Conf. and Exhibition, Vol. 11: Wind Energy, American Society of Mechanical Engineers, Rotterdam, Netherlands, 2022, p.GT2022-83219, V011T38A021. doi: 10.1115/GT2022-83219
28. Fan, J., Huang, J., Yan, J., et al. (2025), *Research on the tension characteristics of a buoy-mooring line system with seabed contact*, Arch. Appl. Mech. 95(10): 241. doi: 10.1007/s00419-025-02951-z
29. Abad, L.R.N., Zareei, M.R., Ebrahimi, A. (2024), *Investigating the effect of clump weight of mooring lines on the motions of floating structures in the sea*, J Mar. Eng. 20(44): 12-23. doi: 10.61186/marineeng.20.44.2
30. Guo, X., Yang, J., Lu, W., Li, X. (2018), *Dynamic responses of a floating tidal turbine with 6-DOF prescribed floater motions*, Ocean Eng. 165: 426-437. doi: 10.1016/j.oceaneng.2018.07.017

© 2026 The Author. Structural Integrity and Life, Published by DIVK (The Society for Structural Integrity and Life 'Prof. Dr Stojan Sedmak') (http://divk.inovacionicentar.rs/ivk/home.html). This is an open access article distributed under the terms and conditions of the Creative Commons Attribution-NonCommercial-NoDerivatives 4.0 International License